

Novel battery thermal management system with different shapes of pin fins

Zengjia Guo[1], Siyuan Zhao[1], Jian Wang[1], Yang Wang[1], Shuo Zhai[1], Tianshou Zhao[2,*], Meng Ni[1,*]

[1] Department of Building and Real Estate, Research Institute for Sustainable Urban Development (RISUD) and Research Institute for Smart Energy (RISE), The Hong Kong Polytechnic University, Hung Hom, Kowloon, Hong Kong, China

[2] Department of Mechanical and Aerospace Engineering, Hong Kong University of Science and Technology, Hong Kong, China

Corresponding authors: metzhao@ust.hk (T.S. Zhao); meng.ni@polyu.edu.hk (M. Ni)

Abstract: Battery thermal management systems (BTMS) with favorable working performance are essential for lithium-ion battery inside the electrical vehicles. In this research, a novel BTMS is proposed by introducing vertically and horizontally arranged square pin fins (SPFs), circular pin fins (CPFs) and ellipse pin fins (EPFs) into the cold plate. The overall cooling performance (efficiency index: EI) of the proposed BTMS is evaluated numerically, considering both heat transfer and pressure loss. It is found that BTMS with SPFs always achieve the best cooling performance but is penalized with a higher pressure loss. EPFs arranged BTMS can achieve the lowest pressure loss due to the excellent streamlined structure but its cooling performance is also the lowest among these 3 different pin fin shapes. Considering both heat transfer and pressure loss, CPFs can be the best choice for BTMS when pin fins are vertically arranged, due to the favorable cooling performance and acceptable pressure loss caused by CPFs. However, the pressure loss is larger for all horizontally arranged pin fins. Considering both heat transfer and friction factor, SPFs are recommended for BTMS because of the greater enhancement of heat transfer.

Keywords: Battery; Thermal management system; Pin fins; Modeling; Cooling; Pressure loss.

Nomenclature

ρ: Density [kg/m^3]

Q_g: Total generated heat [W]

Q_r: Reaction heat

Q_j: Ohmic heat

Q_p: Polarization heat

I: Discharge current

E_{oc}: Open circuit voltage

R_e: Pure resistance of battery

R_p: Polarization resistance

R_t: Total resistance

V_p: Volume of pin fins

λ: Heat conductivity coefficient [W//m•K]

$\vec{v}$: Velocity vector

P: Pressure [Pa]

D_h: Hydraulic diameter

V_t: Volume of mini-channels without pin fins

Nu: Nusselt number

q: Heat flux

A_f: Effective heat transfer area

f: Friction factor

ΔP: Pressure loss

u: Average velocity

L: Length of mini-channel

Subscripts

b: Battery

c: Cooling medium

m: Mini-channel cold plate

oc: Open circuit

r: Reaction

j: Joule

p: Polarization

Acronyms

BTMS: Battery thermal management system

CPF: Circular pin fin

SPF: Square pin fin

EPF: Ellipse pin fin

EI: Efficiency index

UDF: User defined function

1. Introduction

1.1. Review of Lithium-ion battery thermal management system (BTMS)

Lithium-ion (Li-ion) battery is an effective method of energy storage, which is widely used in electric vehicles[1]. However, the significant heat generated inside the Li-ion battery during working process can substantially influence the electrochemical performance, life, reliability, and safety. According to the research[2-4], Li-ion battery can only achieve the best working performance when temperature is controlled within the range of 15℃-40℃, and the temperature difference in the battery should be below 5℃. Performance reduction, capacity degradation and thermal runaway can be easily observed if working temperature is higher than that range[5]. Therefore, an effective battery thermal management system (BTMS) is the

indispensable part of the battery pack for efficient, stable, and safe operation.

Battery cooling systems are divided into several parts according to different types of working medium, such as air, liquid and phase change materials (PCM). As compared to air cooling and PCM cooling, liquid cooling BTMS is preferred due to its excellent convective thermal conductivity and compactness. Water, the mixture of water and glycol[6], mineral/silicon oil[7], nanofluid[8, 9], and liquid metal[10] have been used as the coolant to directly cool the battery pack. To reduce the risk of leakage and corrosion, the cold plate is introduced into liquid cooling BTMS. The working performance of liquid cooling BTMS with cold plate is directly affected by flow path design such as serpentine type[11], U-turn type[12], Z-turn type[13] and so on. However, poor heat transfer performance was observed in the area around the outlet, which is due to the too-long flow path. This adverse effect could be avoided by using the mini-channel cold plate[14]. Wang[15] designed the orthogonal test and determined optimal parameters of mini-channel cold plate. Qian[16] found that BTMS always have the optimum inlet flow rate, considering both maximum temperature and pressure loss. In addition, channel number, flow direction, cold plate thickness, mini-channel width and the shape of mini-channel had also been extensively investigated to obtain the favorable thermal behaviors with acceptable pressure loss[17-19].

However, it is unavoidable for liquid cooling BTMS that the thickness of the thermal boundary layer will gradually increase as the coolant flows, leading to the deterioration in cooling performance [20]. Therefore, new BTMS designs that can improve heat transfer and reduce temperature gradients are needed for effective BTMS. Jin[21] proposed a cold plate with oblique fins which could periodically redevelop the boundary layer, achieving better cooling performance with acceptable pressure loss. Nur[22] investigated the effect of oblique fin arrangement and observed better performance of louvered arrangement than inline and incline arrangement. Mohammed[23] added staggered circular pins into the cold plate to

achieve more effective heat transfer performance. Xu[24, 25] optimized cold plate splitter structure parameters by experiments and numerical simulations, enhancing the thermal equilibrium of the battery pack.

1.2. Research gap and new contribution of this study

The roughed elements which can increase the turbulent intensity and induce the vortexes have achieved good results in the liquid cooling BTMS by disturbing coolant, redeveloping boundary layer and changing liquid flow state. However, little research has been focused on the implementation of roughed elements inside the mini-channel cold plate, and even fewer researchers have focused on the roughed elements shape. It is still unknown how will the different roughed elements affect the temperature of the batteries as well as the friction factor of BTMS. Therefore, the novel mini-channel cold plates with three different shapes of pin fins were proposed and numerically evaluated in this study, including circular pin fin (CPF), square pin fin (SPF) and ellipse pin fin (EPF). Three-dimensional (3D) numerical computations were conducted to fully characterize the fluid flow and heat transfer properties of BTMS. Efficiency index (*EI*) was introduced as an indicator to fully consider both heat transfer performance and pressure loss. The performance comparisons were made to identify suitable pin fins for BTMS with mini-channel cold plate under high discharge rate. In addition, the effects of layout direction of pin fins on the performance of BTMS was also analyzed, due to the significant effects of different layout directions on the heat transfer performance and friction factor.

2 Numerical model

2.1 The Geometry

In this research, a typical battery pack with 5 batteries is employed and every single battery is sandwiched by two mini-channel cold plates. The Li-ion battery (LIB) is rectangular-shaped with the size of 128 mm length, 79 mm width, and 12 mm height. The anode and cathode materials are $LiFePO_4$ and graphite. The current taps are made of Al and Cu, and the length

and width are 10 mm and 9 mm respectively with a height of 4 mm. The specifications of LIB are shown in Table 1.

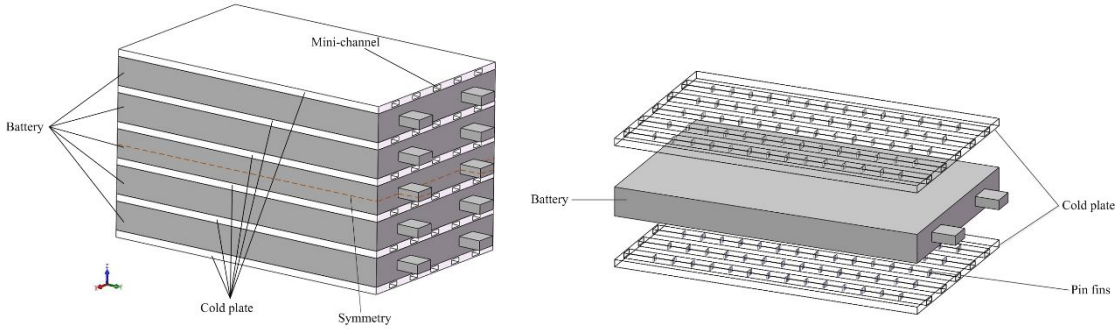

Fig.1 Schematic diagram of battery pack (a), single battery and mini-channel cold plates with pin fins

Table 1 Thermophysical properties of LIB, cold plate and cooling medium

Content	Battery	Cold plate	Cooling medium
Density(kg/m^3)	1969.59	2719	998.2
Specific heat(J/kg•K)	1305	871	4182
Thermal conductivity (W/m•K)	$\lambda_x = \lambda_y$ =23.7 λ_z = 3.6	202.4	0.6
Viscosity(kg/m•s)	N/A	N/A	0.001003

Fig.1(b) shows the single battery and mini-channel cold plates. The cold plates have the same length and width as the LIB, with a height of 3mm. The number of mini-channels is considered to be 5 due to favorable cooling performance and pressure loss according to our previous simulation results. The mini-channels are uniformly distributed inside the cold plate with a length of 128mm, width of 5mm, and height of 2mm. The cold plates and pin fins are made of Al, and liquid water is chosen as the cooling medium. The thermophysical properties of the cold plate and cooling medium are also listed in Table 1.

Fig.2 shows the pin fins shapes and pin fins arrangements. It can be easily found that the efficient heat exchange area and available volume of the mini-channels are variable when

different pin fins are arranged, which have a huge effect on the working performance of mini-channels. Therefore, the hydraulic diameter of the mini-channel is adopted to form a basis for comparing the performance of the BTMS with different pin fins (Table 2). Pin fins are staggered arranged in totally14 rows, with 12mm between the first row of pin fins and the inlet as well as the last row of pin fins and the outlet. Streamwise and spanwise spacings between the centers of neighboring pin fins are kept at 8mm and 1mm for vertically arranged pin fins, 8mm and 0.4mm for horizontally arranged pin fins respectively. The specific parameters of pin fins are shown in Table 2.

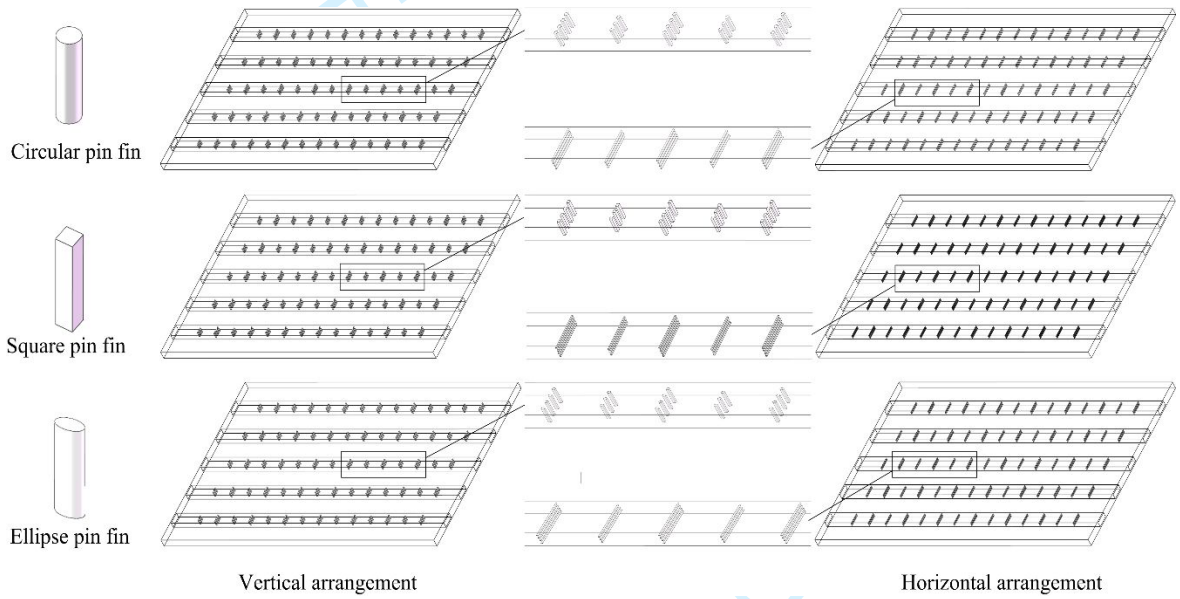

Fig.2 Schematic of pin fins shape and pin fins arrangement

Table 2 Geometrical parameters of differently shaped pin fins

		Diameter/Length (mm)	Hydraulic diameter
Circular pin fins	Vertical arrangement	0.5	2.62
	Horizontal arrangement	0.2	2.62
Square pin fins	Vertical arrangement	0.4	2.62
	Horizontal arrangement	0.16	2.62

Ellipse pin fins	Vertical arrangement	Long axis	0.5	2.66
		Short axis	0.3	
	Horizontal arrangement	Long axis	0.2	2.66
		Short axis	0.12	

2.2 Mathematical model

2.2.1 Governing equations

During charging and discharging, batteries generate a lot of heat and the temperature of batteries can be described as follows:

$$\rho c_p \frac{\partial T}{\partial \tau} = \frac{\partial}{\partial x}(\lambda_x \frac{\partial T}{\partial x}) + \frac{\partial}{\partial y}(\lambda_y \frac{\partial T}{\partial y}) + \frac{\partial}{\partial z}(\lambda_z \frac{\partial T}{\partial z}) + Q_g \quad (1)$$

Where ρ and c_p are the battery density and specific heat capacity; λ_x, λ_y, and λ_z represent the heat conductivity coefficient; Q_g is the total generated heat. The total generated heat is divided into reaction heat (Q_r), ohmic heat (Q_j), and polarization heat (Q_p):

$$Q_r = -IT_b \frac{dE_{oc}}{dT_b} \quad (2)$$

$$Q_j = I^2 R_e \quad (3)$$

$$Q_p = I^2 R_p = I^2 (R_t - R_e) \quad (4)$$

Where I is the current, E_{oc} is the open circuit voltage, T_b is the battery temperature. R_e is the pure resistance, R_t stands for the total resistance, R_p represents polarization resistance.

The energy conservation equations of BTMS are as follows:

$$\rho_c \frac{\partial T_c}{\partial t} + \nabla (\rho_c \vec{v} T_c) = \nabla(\frac{\lambda_c}{c_c} \nabla T_c) \quad (5)$$

$$P_m \frac{\partial T_m}{\partial t} = \nabla(\frac{\lambda_m}{c_m} \nabla T_m) \quad (6)$$

Where ρ, T, c, and λ represents density, temperature, heat capacity, and thermal conductivity; $\vec{v}$ is velocity vector of cooling medium.

The continuity and momentum conservation equations of cooling medium can be described as follows:

$$\frac{\partial \rho_c}{\partial t} + \nabla (\rho_c \vec{v}) = 0 \tag{7}$$

$$\frac{\partial}{\partial t}(\rho_c \vec{v}) + \nabla (\rho_c \vec{v} \vec{v}) = - \nabla P \tag{8}$$

Where P represents static pressure.

2.2.2 Parameter definition

The hydraulic diameter of the mini-channel is defined as[26]:

$$D_h = \frac{4 (V_t - V_p)}{A_f} \tag{9}$$

Where V_t presents the volume of mini-channel, V_p presents the volume of the pin fins, A_f is the effective heat transfer area.

The overall averaged Nusselt number of the battery pack is defined as[27]:

$$\overline{Nu} = \frac{qD_h}{\lambda_c(T_{ave} - T_c)} \tag{10}$$

Where T_{ave} is the average temperature, q presents the heat flux from the heat transfer area with the cold plate.

Pressure loss is another critical factor for evaluating the system performance of liquid cooling BTMS. The pressure loss characteristics could be represented by the friction factor f[27]:

$$f = \frac{2 \Delta P D_h}{\rho u^2 L} \tag{11}$$

Where ΔP is pressure loss, and u is average velocity, and L is the length of the mini-channel.

In the investigation of cooling performance of BTMS, efficiency index (EI)[28] is calculated to identify the optimal design. EI is an overall evaluation of cooling performance considering both heat transfer and pressure loss:

$$EI = \frac{\overline{Nu}/\overline{Nu_0}}{\left(f/f_0\right)^{1/3}} \quad (12)$$

Where $\overline{Nu_0}$ and f_0 are the Nusselt number and friction factor of the cold plate without pin fins. f/f_0 is the normalized friction factor.

2.3 Boundary conditions

The numerical simulations were performed by using commercial software ANSYS Fluent 19.0. The pressure-velocity coupled solver and the second-order upwind volume discretization scheme were employed. The continuity equation as well as the velocity and turbulence quantity equations were computed till a minimum convergence criterion of 10^{-6} was reached. The standard k-ε model and laminar model were respectively employed in the simulation depending on the Reynolds number.

The mass flow inlet rates ranged from 0.001kg/s to 0.005kg/s with a temperature of 303K was used for the inlet, due to the favorable performance in controlling temperature. The outlet followed a pressure outlet boundary condition with a value of standard atmospheric pressure, and the symmetric boundary condition was used for the battery pack. The side surfaces of the battery pack and cold plates were considered as the free convection, and the heat transfer coefficient was defined as 5 W/(m•K). The discharge rate of LIB was assumed at 9C rate, and the heat source was defined by UDF (user defined function) which considered the reaction heat, ohmic heat and polarization heat to provide the accurate heat generation rate and obtain the reliable results. In addition, the no-slip boundary was also applied.

2.4 Mesh generation and independence verification

The structured hexahedral mesh was generated for all the computation cases, and the cell orthogonally was ensured by the introduction of multiple O-gird type blocks for all CPFs and EPFs. Grid independence check was performed for each computation grid system with the mesh numbers ranging from about 2.5 million to 12.6 million. Fig.3 (a) presents the maximum

temperature and pressure loss of battery pack with CPFs arranged BTMS, when mass flow rate was chosen as 0.003kg/s. With the increase in the total grid number, the computation results became to be invariable and the changes in the maximum temperature and pressure loss are less than 0.03% and 1%. Considering the quality of girds and numerical accuracy, a mesh number of about 8.4 million was chosen, as shown in Fig.3 (b).

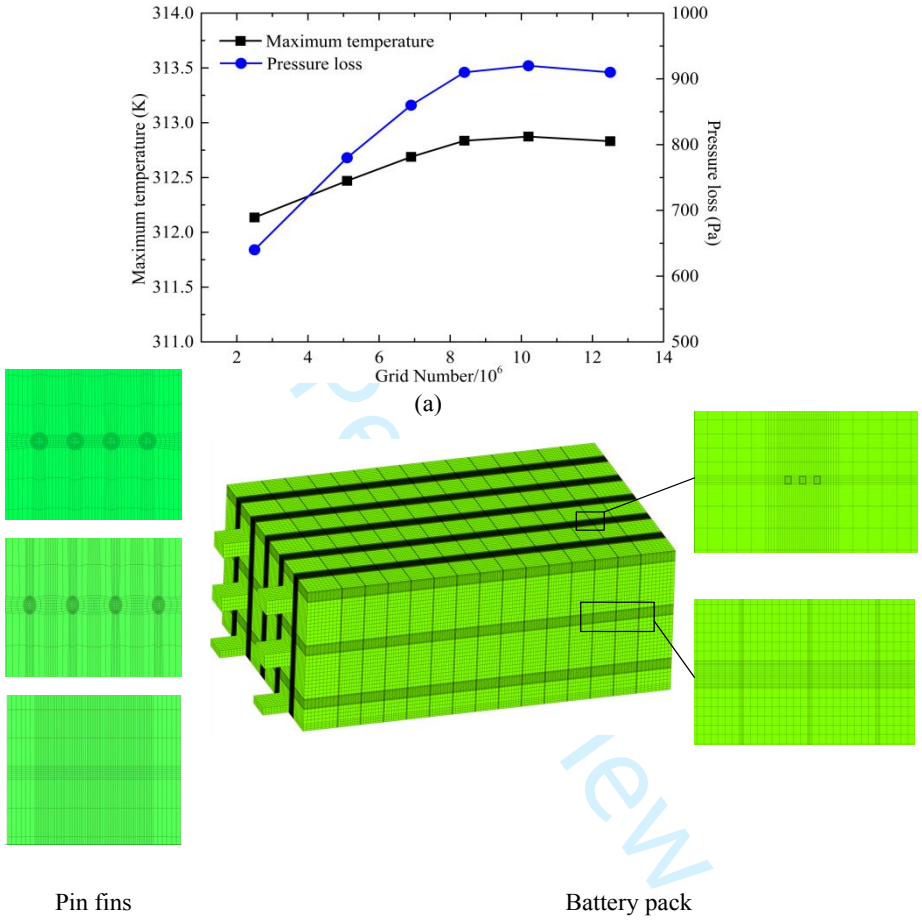

Fig.3 Grid independence verification (a), schematic mesh of battery pack (b)

3 Results and discussion

3.1 Model verification

In order to verify the accuracy of the numerical model used in the simulations, a comparison between the presented maximum temperature and the data by Qian[16] and Rao[29] was performed. Fig.4 shows the maximum temperature of battery pack with no battery thermal

management system when the discharge rate was chosen as 5C. The data deviations on maximum temperature were less than 0.38K and 0.52K respectively, which were considered acceptable. Therefore, the presented data showed good agreement with the data from the literature, and the numerical model used in the simulations was reliable.

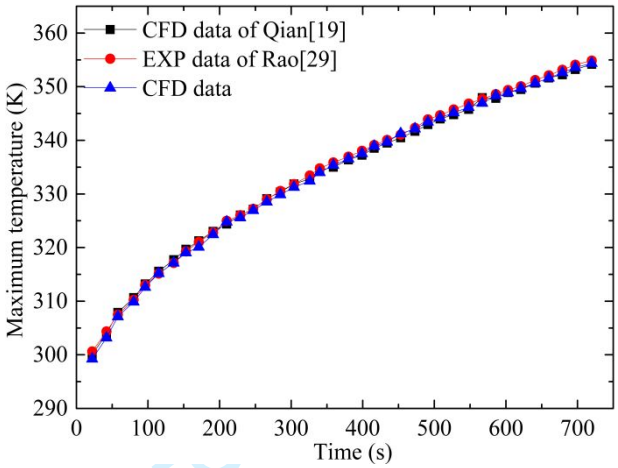

Fig.4 Comparison of present numerical result with published numerical and experimental results

3.2 The effect of vertically arranged pin fins

In order to investigate the differences between the effect of CPFs, SPFs and EPFs on BTMS, numerical simulations were conducted under various mass flow rates to obtain the maximum temperature and maximum temperature difference of battery pack, the maximum temperature difference of single battery, and average heat flux of mini-channels. Fig.5 (a) presents the maximum temperature of the battery pack with differently shaped pin fins at the end of 9C discharge. The maximum temperature in all the cases decreased with the increasing mass flow rate and the pin fins arranged BTMS always achieved better cooling performance than BTMS without pin fins. As mass flow rate changed from 0.001kg/s to 0.005kg/s, the battery pack with SPFs arranged BTMS achieved the lowest maximum temperature, which was 2.01K, 1.83K, 1.67K, 1.48K and 1.32K lower than that of EPFs arranged BTMS, 1.16K, 1.08K, 1.01K, 0.91K and 0.84K lower than that of CPFs arranged BTMS. In addition, the BTMS without pin fins could only cool down the maximum temperature to below 313K at a high mass

flow rate of 0.005 kg/s. For comparison, only 0.004 kg/s was needed for the battery pack with EPFs, and 0.003 kg/s was needed for the battery pack with CPFs and SPFs.

For all the cases, the maximum temperature difference decreased with increasing mass flow rate, as shown in Fig.5 (b) and Fig.5 (c). The maximum temperature difference within both single battery and battery pack was obviously reduced, due to the implementation of pin fins, especially SPFs. When mass flow rate ranged between 0.001kg/s and 0.005kg/s, the maximum temperature difference of single battery with SPFs arranged BTMS was lowered by 1.15K, 0.99K, 0.85K, 0.74K, and 0.67K as compared to BTMS with EPFs, and by 0.46K, 0.38K, 0.29K, 0.26K and 0.22K as compared to BTMS with CPFs. The maximum temperature difference of battery pack with SPFs arranged BTMS was lowered by 1.47K, 1.28K, 1.12K, 1.02K and 0.88K as compared to BTMS with EPFs, and by 0.68K, 0.60K, 0.51K, 0.47K and 0.42K as compared to BTMS with CPFs. Besides, 0.003kg/s and 0.004kg/s mass flow rates were needed to control the maximum temperature difference of single battery and battery pack within 5K when SPFs arranged BTMS was used. But BTMS with CPFs and EPFs needed higher mass flow rates and BTMS without pin fins could never reach this temperature difference under the investigated mass flow rates.

Fig.5 (d) shows the average heat flux of mini-channel under the various mass flow rates. It can be observed that the average heat fluxes of all the pin fins arranged BTMS were higher than that of BTMS without pin fins. It was also found that the BTMS with differently shaped pin fins had the different average heat flux. SPFs arranged BTMS achieved the highest average heat flux, leading to the best heat transfer performance and temperature distribution. It was higher than that of EPFs arranged BTMS by 8.8%, 8.5%, 7.6%, 6.4% and 6.1%, than that of CPFs arranged BTMS by 4.8%, 4.8%, 4.4%, 3.8% and 3.7%, at mass flow rate from 0.001kg/s to 0.005kg/s.

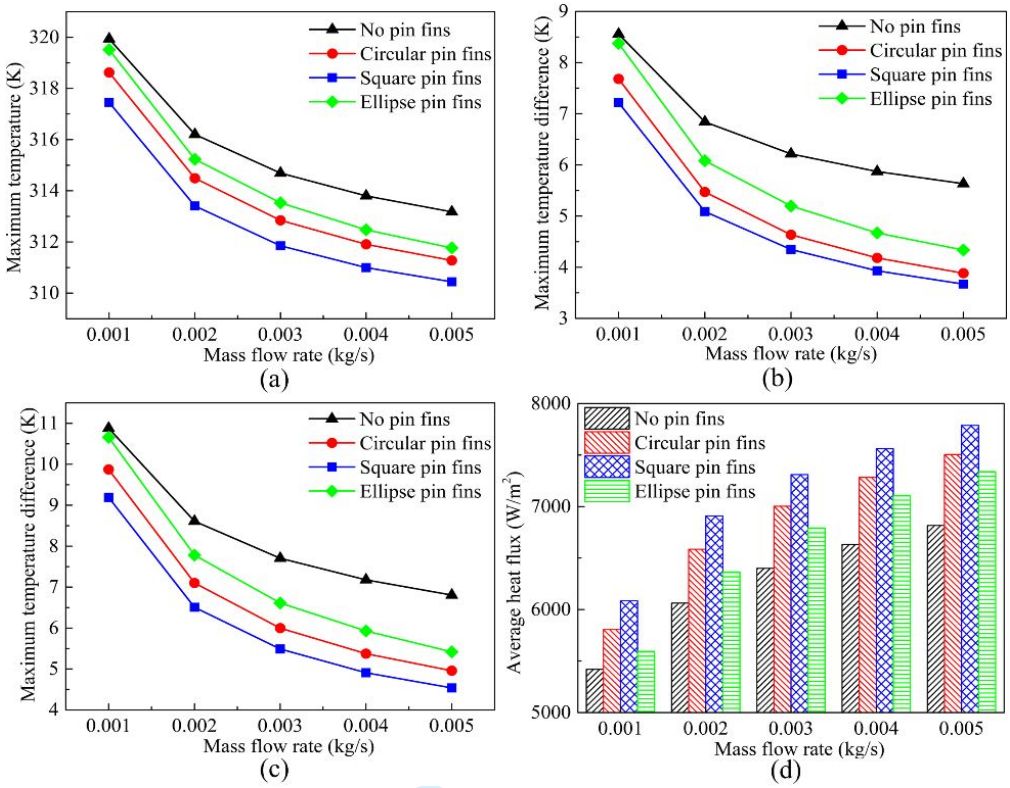

Fig.5 Maximum temperature of battery pack (a), maximum temperature difference within single battery (b), maximum temperature difference within battery pack (c), average heat flux of mini-channel (d)

Fig.6 depicts the temperature distribution of the battery pack. Increasing mass flow rate was helpful to achieve a better temperature distribution for all the designs. The highest temperature of every single battery appeared around the intermediate area, and the maximum temperature of battery pack appeared at the central section of cell 3. The high temperature region was moving slowly to the center area as the mass flow rate increases.

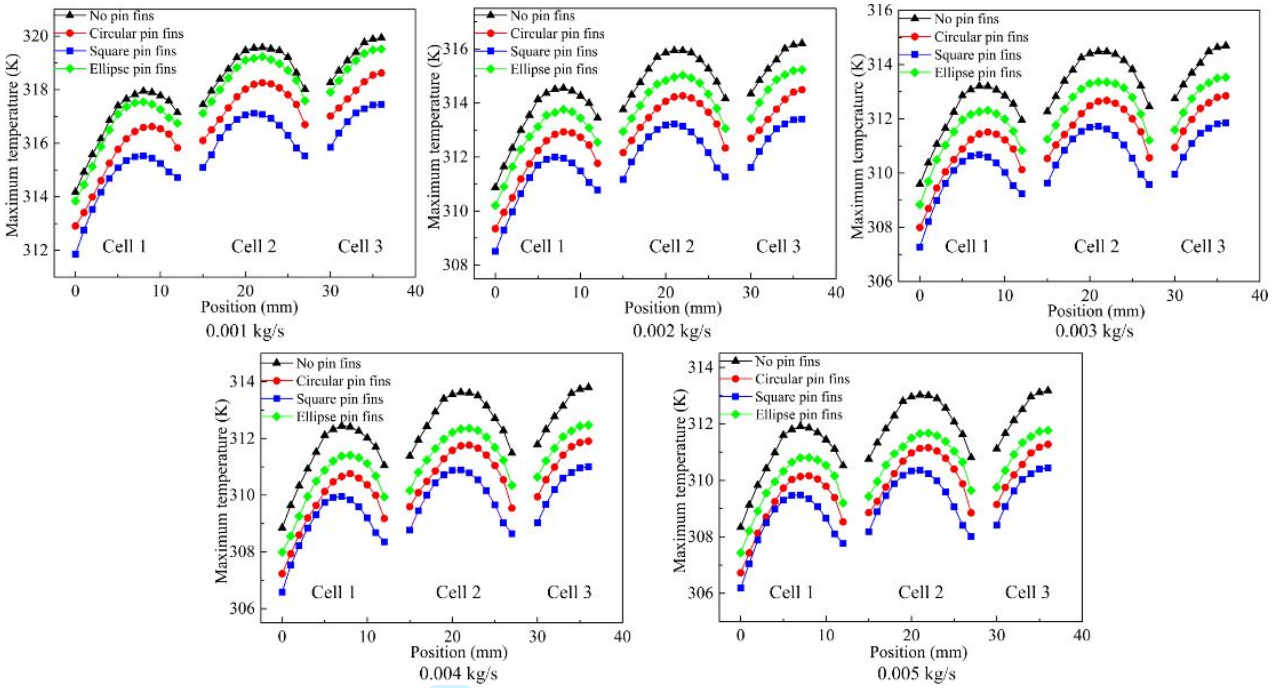

Fig.6 Max temperature distribution along Z-direction

In liquid cooling BTMS, the implementation of pin fins can be penalized by the adverse effect of pressure loss. Thus, pressure loss must be considered for the evaluation of the BTMS. Hence, the optimal goal of the BTMS design is to achieve a better heat transfer with acceptable pressure loss. Fig.7 respectively shows the pressure loss and normalized friction factor of the BTMS with CPFs, SPFs, EPFs and without pin fins. It can be observed that all values of normalized friction factor exceeded 1, which implied that pin fins would increase the extra pressure loss in the BTMS. The pressure loss and normalized friction factor in all the cases increased with increasing mass flow rates, but the increment in the normalized friction factor became smaller and smaller. Under the investigated mass flow rates, the SPFs caused the highest normalized friction factor, which was higher than that of CPFs by 0.9, 1.02, 1.05, 1.07 and 1.07, than that of EPFs by 1.01, 1.12, 1.15, 1.15 and 1.15.

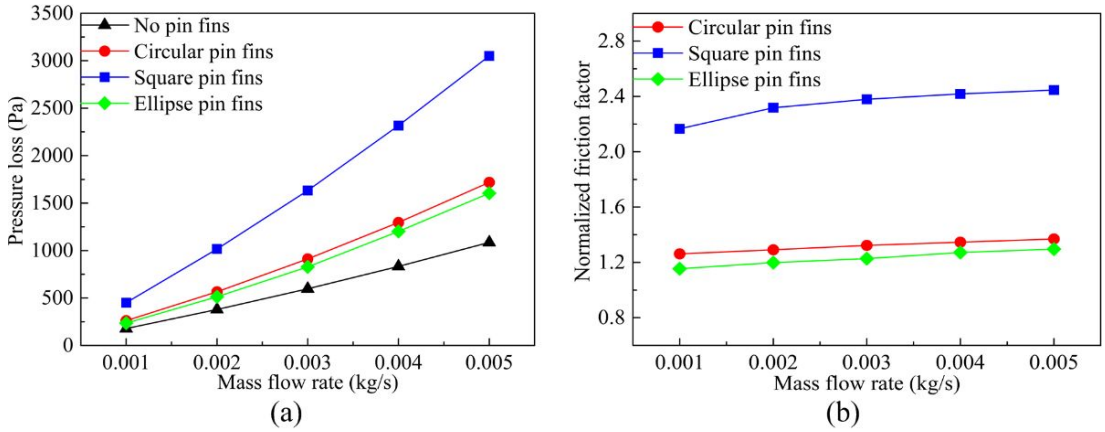

Fig.7 Pressure drop (a), and normalized friction factor (b) of BTMS with differently shaped pin fins

It is known that the impingement of coolant on the pin fins surface could refresh the boundary layer development and transform the laminar flow into the turbulent flow, leading to a favorable heat transfer performance. However, totally different turbulent intensity and flow characteristics can be observed in the mini-channel of BTMS with CPFs, SPFs and EPFs, as shown in Fig.8. Firstly, the turbulent intensity and coolant velocity in all the cases increased with increasing mass flow rate. Besides, high coolant velocity with strong turbulence was always observed on both sides of the mini-channel for these three designs because of the effect of pin fins. But SPFs arranged BTMS had the strongest turbulent intensity and the highest flow velocity. The ability of CPFs in enhancing turbulent intensity and flow velocity was only stronger than that of EPFs.

As for SPFs arranged BTMS, there were a lot of small-scale vortexes generated inside the mini-channel, and obvious large-scale vortexes were observed on both sides of the mini-channel. As a result, the strong turbulent intensity with favorable distribution was generated in the mini-channel. Therefore, the heat transfer performance and temperature distribution were significantly improved, but the adverse effect of high pressure loss was inevitable. Due to the excellent streamlined structure of EPFs, there was little high intensity turbulence generated when coolant flowing through EPFs. Therefore, only several strong turbulent intensity areas

could be observed in the mini-channel except on both sides. While this flow characteristic inside the EPFs arranged BTMS could reduce the generation of extra pressure loss, it also limits the ability of enhancing heat transfer. As for CPFs arranged BTMS, although several low turbulent intensity areas still existed, the strong turbulent intensity areas still occupied most areas of the mini-channel. The distribution of turbulence intensity is also relatively uniform inside the mini-channel. Therefore, the higher pressure loss could be caused by CPFs, but the heat transfer performance was improved and the temperature distribution was also well optimized.

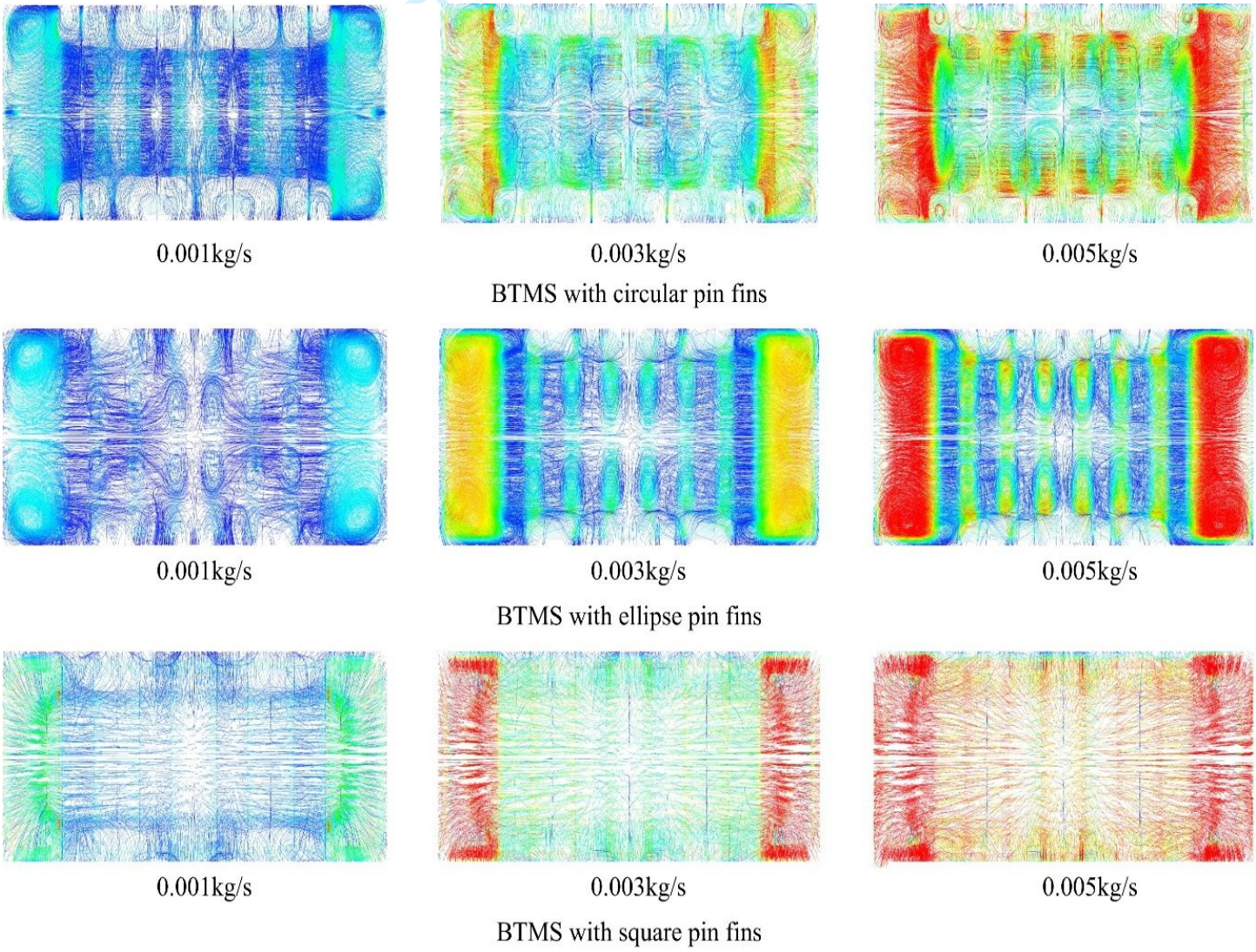

Fig.8 Streamlines distribution in mini-channel with differently shaped pin fins

To further evaluate the cooling performance of the BTMS with pin fins, efficiency index

(*EI*) was calculated for each result obtained in this study. Higher *EI* implies more favorable overall cooling performance with high heat transfer performance and acceptable pressure loss. Fig.9 depicts the *EI* of BTMS with differently shaped pin fins. It can be observed that the cases of SPFs and CPFs arranged BTMS always exhibit *EI* greater than 1, indicating that the implementation of SPFs and CPFs enhanced heat transfer with acceptable friction factor increment. It means that SPFs and CPFs could always improve the overall cooling performance of the BTMS under the investigated mass flow rates. However, as for EPFs arranged BTMS, the *EI* value was lower than 1 when the mass flow rate was 0.001kg/s, which is due to the bad performance in improving heat transfer. It means that the adverse effect of extra pressure loss caused by EPFs was more serious than the effect of heat transfer enhancement. Therefore, EPFs were not favorable to improving the overall cooling performance of BTMS when the mass flow rate was chosen as 0.001kg/s. But as mass flow rates varying between 0.002kg/s and 0.005kg/s, EPFs arranged BTMS could exhibit *EI* greater than 1, indicating that EPFs could enhance the overall cooling performance of BTMS at a high mass flow rate.

Fig.9 also presents that the *EI* value of all these three designs increased with increasing mass flow rate, but the increment in *EI* became smaller and smaller. As the mass flow rate increasing from 0.001kg/s to 0.005kg/s, the CPFs arranged BTMS always achieved the highest *EI*, which was higher than that of SPFs arranged BTMS by 0.012, 0.014, 0.022, 0.029 and 0.034, higher than that of EPFs arranged BTMS by 0.069, 0.095, 0.112, 0.114 and 0.119. Therefore, considering both heat transfer performance and pressure drop, CPFs can be the best choice from the other pin fins when pin fins were vertically arranged inside the BTMS.

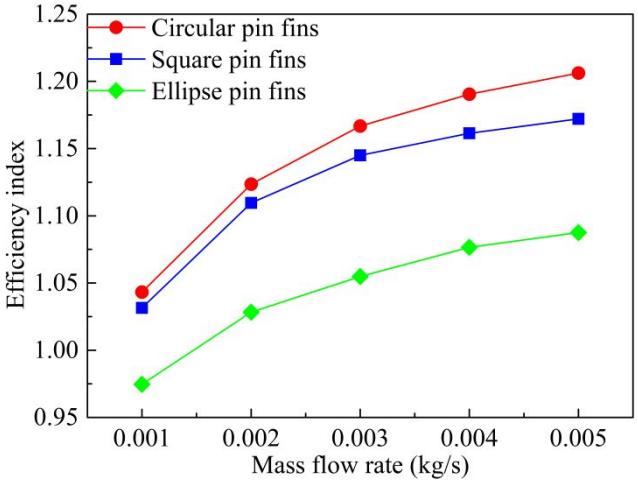

Fig.9 Efficiency index of BTMS with differently shaped pin fins

3.3 The effect of horizontally arranged pin fins

The flow structures in mini-channel are distinctly different when different pin fins layout directions are used, leading to the different heat transfer performance and friction factor. Thus, the differently shaped pin fins have different effects on improving the overall cooling performance of BTMS when pin fins are arranged in different layout directions. However, such study has not been reported for BTMS with pin fins yet. Therefore, in order to investigate the effect of horizontally arranged CPFs, SPFs and EPFs on BTMS, numerical simulations were conducted under various mass flow rates.

Fig.10 (a), Fig.10 (b), and Fig.10 (c) present the maximum temperature of battery pack, maximum temperature difference within single battery and battery pack, respectively. The BTMS with horizontally arranged pin fins also achieved the lower maximum temperature of battery pack than BTMS without pin fins. As mass flow rate increasing from 0.001kg/s to 0.005kg/s, BTMS with SPFs achieved the lowest maximum temperature of the battery pack, which was lowered by 5.77K, 3.27K, 2.48K, 2.08K and 1.91K as compared to the BTMS with EPFs, 3.54K, 1.85K, 1.25K, 0.96K and 0.82K as compared to the BTMS with CPFs. In addition, lower mass flow rate was needed for BTMS with horizontally arranged pin fins to control the maximum temperature of battery pack below 313K than BTMS with vertically arranged pin

fins.

In addition, the maximum temperature differences of single battery and battery pack with EPFs arranged BTMS were higher than that of BTMS without pin fins when mass flow rate was 0.001kg/s and 0.002kg/s. Only when mass flow rate was higher than 0.003kg/s, these two parameters were lower than that of BTMS without pin fins. However, SPFs and CPFs arranged BTMS always achieve lower temperature difference within single battery and battery pack than BTMS without pin fins. The BTMS with SPFs achieved the lowest maximum temperature difference within single battery, which was 1.95K, 1.08K, 1.01K, 0.79K and 0.78K lower than that of BTMS with EPFs, 0.81K, 0.55K, 0.52K, 0.39K, and 0.35K lower than that of BTMS with CPFs. The lowest maximum temperature difference within battery pack was also achieved by BTMS with SPFs, which was 3.88K, 2.5K, 1.83K, 1.51K and 1.36K lower than that of BTMS with EPFs, 1.92K, 1.27K, 0.83K, 0.62K and 0.49K lower than that of BTMS with CPFs. In addition, the BTMS with horizontally arranged pin fins needed higher mass flow rate than BTMS with vertically arranged pin fins to control the maximum temperature difference of single battery and battery pack within 5K. Fig.10 (d) presents the average heat flux of mini-channels. It can be observed that the BTMS with SPFs showed the highest average heat flux, and the average heat flux of BTMS with CPFs was lower than that of BTMS with SPFs but higher than that of BTMS with EPFs.

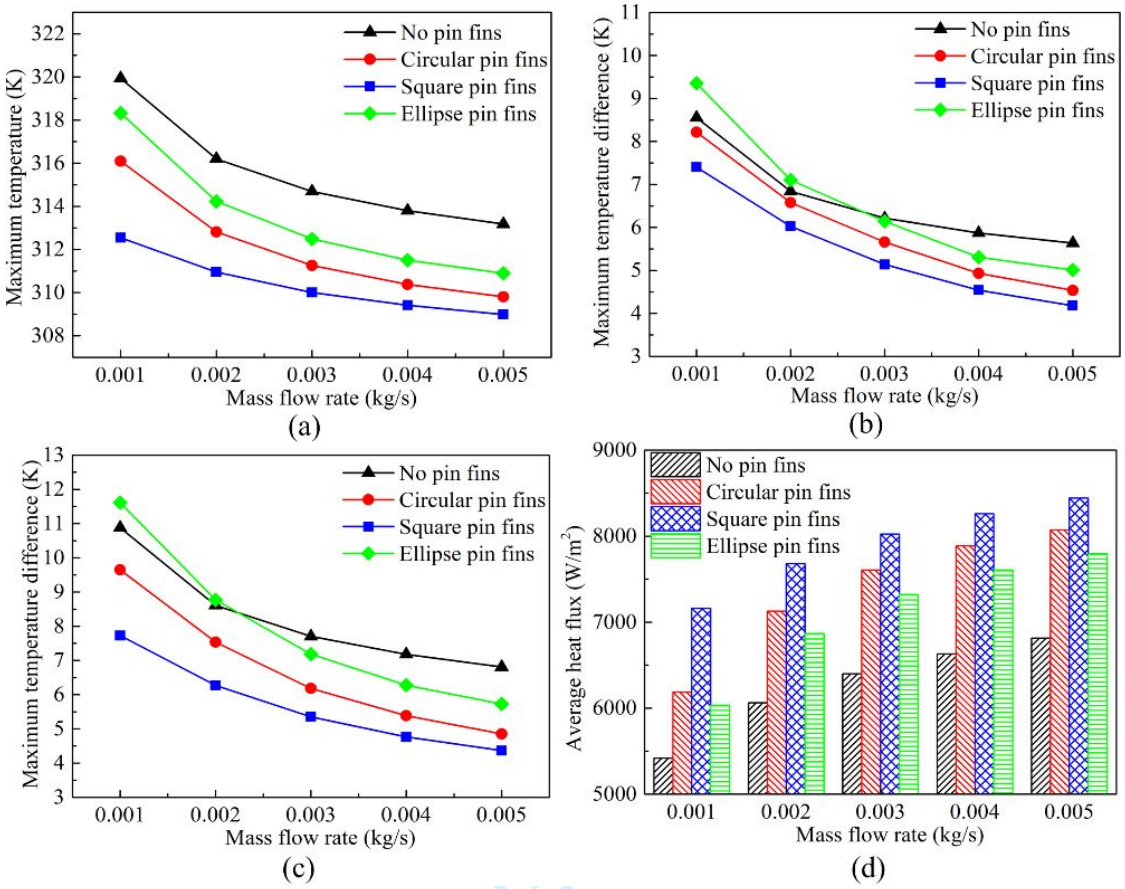

Fig.10 Maximum temperature of battery pack (a), maximum temperature difference within single battery (b), maximum temperature difference within battery pack (c), average heat flux of mini-channel (d)

Fig.11 presents the maximum temperature distribution along Z-direction. Increasing mass flow rate can achieve the better temperature distribution for all designs. It can be observed that the temperature around the intermediate area was always higher than the temperature in the two sides of every single battery and the maximum temperature of the battery pack appeared at the central section of cell 3. Battery pack with horizontally arranged SPFs, CPFs and EPFs showed the similar changing trend, which was different from the BTMS with vertically arranged pin fins. The highest temperature of every single battery appeared at the central part instead of the right part, and cell 2 and cell 3 had the similar temperature distribution.

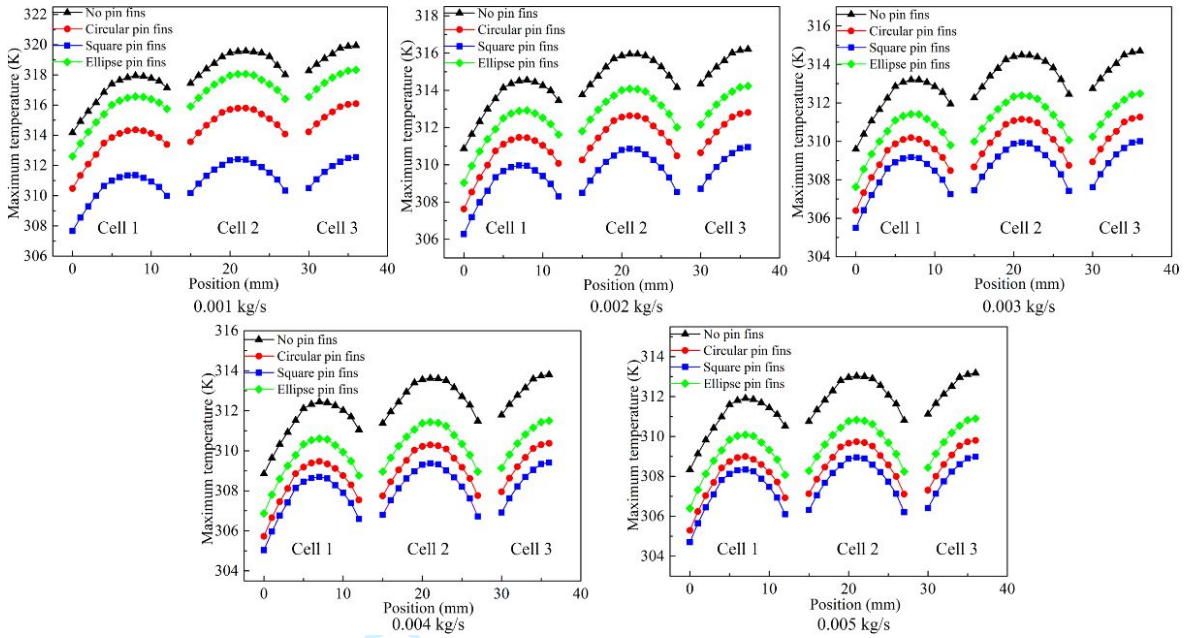

Fig.11 Max temperature distribution along Z-direction

Fig.12 shows the pressure loss and normalized friction factor of BTMS, respectively. The pressure loss and normalized friction factor increased with the increasing mass flow rates, and the increment in normalized friction factor became smaller and smaller. When pin fins were horizontally arranged, SPFs still caused the highest normalized friction factor, which was higher than that of CPFs by 1.94, 1.87, 1.29, 0.96 and 0.91, than that of EPFs by 2.42, 2.79, 2.65, 2.52 and 2.59.

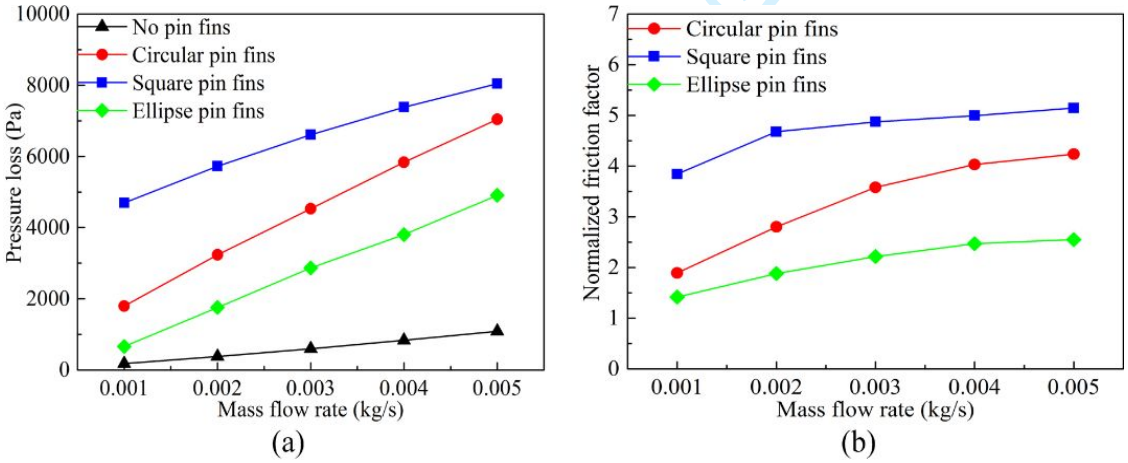

Fig.12 Pressure drop (a), and normalized friction factor (b) of BTMS with differently shaped pin fins

Fig.13 shows the streamlines distribution of mini-channel cross-section under different

mass flow rates, indicating that horizontally arranged pin fins produced distinctly different flow structures with vertically arranged pin fins. Due to the small height of mini-channels, there was a strong interaction between the coolants as the coolant passing through the horizontally arranged pin fins, leading to intense turbulence. The large-scale vortexes were generated in the mini-channel due to the horizontally arranged pin fins. Especially at the top and bottom of the mini-channel, the flow velocities and intensity of turbulence were extremely high, but the high extra pressure loss was also generated inevitably.

In addition, SPFs, CPFs and EPFs arranged BTMS produced different flow characteristics with each other. Among these three kinds of pin fins, SPFs had the strongest ability in enhancing turbulent intensity and flow velocity. The ability of CPFs was weaker than SPFs but stronger than EPFs. As for SPFs arranged BTMS, the obvious large-scale vortex with the highest intensity turbulence could always be observed inside the mini-channel even under the low mass flow rate. Therefore, the cooling performance and temperature distribution were greatly improved. However, the heat transfer enhancement was accompanied by the highest pressure loss. Even though EPFs had the excellent streamlined structure, the high intensity turbulence and large-scale vortexes were still generated due to the horizontal arrangement of pin fins. In addition, a lot of small-scale vortexes could also be observed inside the mini-channel. Therefore, BTMS with horizontally arranged EPFs could achieve better heat transfer performance. As for BTMS with CPFs, there were some low turbulent intensity areas inside the mini-channel, especially in the center part of the mini-channel. However, the large-scale vortexes with high intensity turbulence appeared at the top and bottom of mini-channel, which played the dominant role in enhancing heat transfer performance and producing pressure loss. Therefore, favorable heat transfer performance was achieved by CPFs arranged BTMS, as well as the high pressure loss.

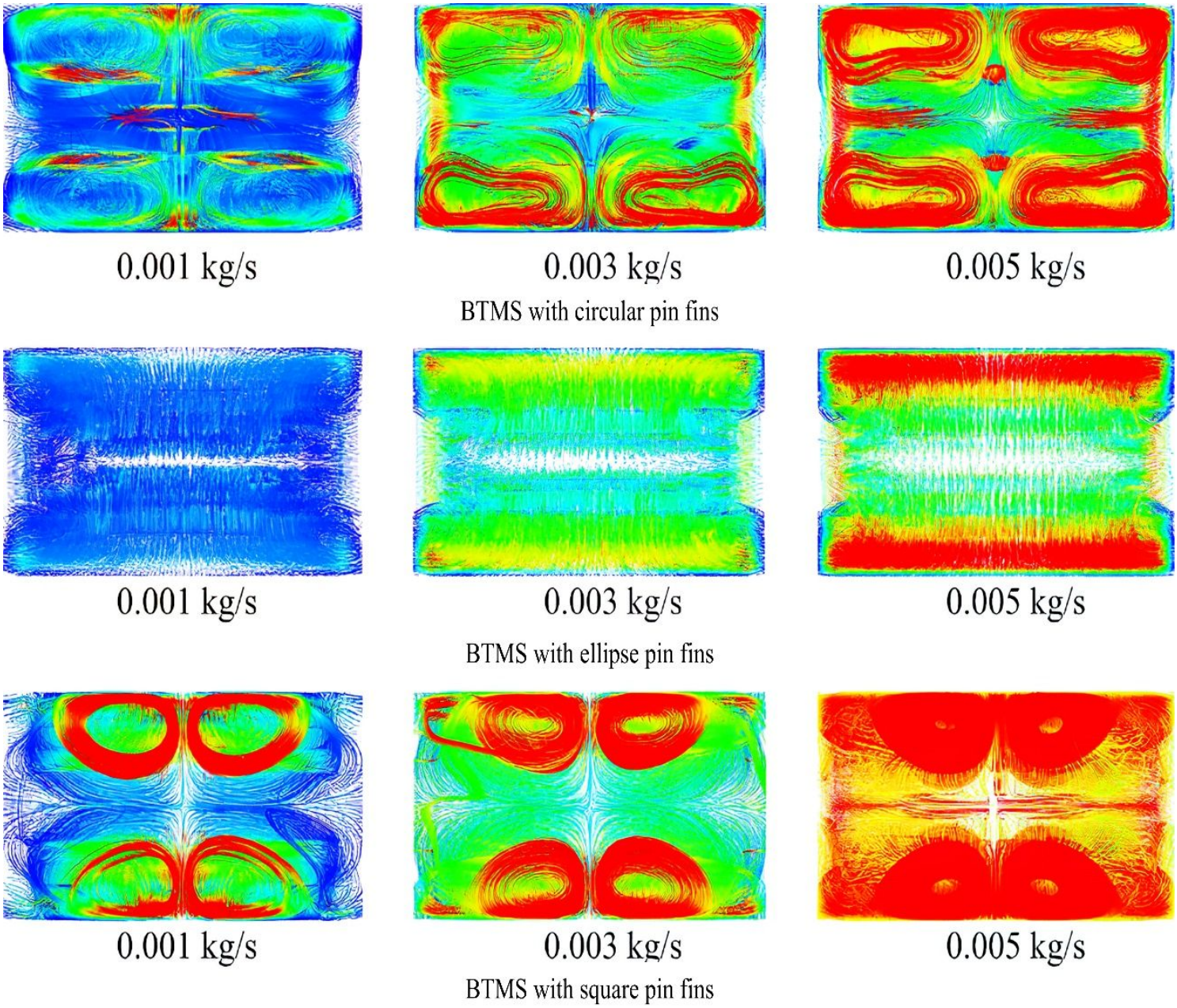

Fig.13 Streamlines distribution in mini-channel with differently shaped pin fins

Fig.14 shows the *EI* of BTMS with SPFs, CPFs and EPFs under the different mass flow rates. It can be observed that all cases exhibited *EI* greater than 1, indicating that horizontally arranged SPFs, CPFs and EPFs could improve the overall cooling performance of the BTMS under all the investigated mass flow rates. It means that although horizontally arranged pin fins caused extremely high pressure loss, the heat transfer enhancement could bring more benefits to the BTMS.

In addition, *EI* of BTMS with horizontally arranged pin fins decreased with the increasing mass flow rate. Under the investigated mass flow rates, the SPFs arranged BTMS always achieved the highest *EI*, which was higher than that of CPFs arranged BTMS by 0.143, 0.146, 0.142, 0.141 and 0.141, higher than that of EPFs arranged BTMS by 0.199, 0.202, 0.201, 0.206 and 0.211. This is because that all the horizontally arranged pin fins caused very high pressure loss. Even though CPFs and EPFs had a better streamlined structure than SPFs, the pressure loss was still not controlled in a reasonable range effectively, and meanwhile the heat transfer enhancement was limited. Therefore, considering the trade-offs between cooling performance and friction factor in the design of BTMS with horizontally arranged pin fins, the SPFs can be the best choice from the other pin fins.

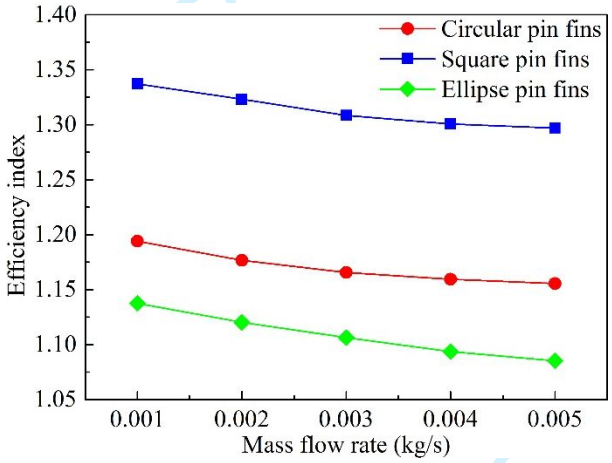

Fig.14 Efficiency index of BTMS with different pin fins

4 Conclusions

In order to investigate the effect of differently shaped pin fins on improving the thermal performance of BTMS for battery pack operating at a high current, numerical simulations were conducted on the BTMS with vertically and horizontally arranged SPFs, CPFs and EPFs in this paper. The effect of SPFs, CPFs and EPFs on the temperature, temperature distribution, pressure drop, and flow structure were systematically studied. The efficiency index was used as an overall indicator, measuring both the thermal behaviors and pressure drop. The conclusions are summarized below:

(1) BTMS with SPFs always achieved the best performance in controlling temperature and temperature difference but also was penalized with the highest pressure loss according to the best ability in enhancing turbulent intensity and generating vortex. CPFs had a lower efficiency of heat transfer improvement than SPFs, but it was better than that of EPFs. However, EPFs caused the lowest pressure loss due to the excellent streamlined structure.

(2) *EI* value of BTMS with vertically arranged pin fins increased with increasing mass flow rate. BTMS with CPFs achieved the highest *EI* value which was higher than that of SPFs arranged BTMS by 0.012, 0.014, 0.022, 0.029 and 0.034, higher than that of EPFs arranged BTMS by 0.069, 0.095, 0.112, 0.114 and 0.119. It is indicated that CPFs could be the best choice to improve the overall cooling performance of BTMS when pin fins were vertically arranged.

(3) *EI* value decreased with increasing mass flow rate when pin fins were horizontally arranged inside BTMS. Due to the horizontal arrangement of pin fins, CPFs and EPFs could no longer control the extra pressure loss within the reasonable range. Therefore, BTMS with horizontally arranged SPFs achieved the highest *EI* which was higher than that of CPFs arranged BTMS by 0.143, 0.146, 0.142, 0.141 and 0.141, higher than that of EPFs arranged BTMS by 0.199, 0.202, 0.201, 0.206 and 0.211.

(4) As mass flow rate ranged from 0.001kg/s to 0.005kg/s, vertically arranged pin fins achieved favorable heat transfer enhancement and acceptable pressure loss. But due to the strong interaction between the coolants as the coolant passing through the pin fins, the horizontally arranged pin fins caused the highest heat transfer enhancement as well as the highest extra pressure loss. Among all the investigated cases, the horizontally arranged SPFs could be the best choice for BTMS as referring to EI value.

Acknowledgement:

This research is supported by a grant under the Theme-based Scheme (project number: T23-

601/17-R) from Research Grant Council, University Grants Committee, Hong Kong SAR.

References

[1] Pesaran AA, Vlahinos A, Burch SD. Thermal performance of EV and HEV battery modules and packs: National Renewable Energy Laboratory; 1997.

[2] Nagasubramanian G. Electrical characteristics of 18650 Li-ion cells at low temperatures. Journal of applied electrochemistry. 2001;31:99-104.

[3] Ramadass P, Haran B, White R, Popov BN. Capacity fade of Sony 18650 cells cycled at elevated temperatures: Part I. Cycling performance. Journal of power sources. 2002;112:606-13.

[4] Jouhara H, Khordehgah N, Serey N, Almahmoud S, Lester SP, Machen D, et al. Applications and thermal management of rechargeable batteries for industrial applications. Energy. 2019;170:849-61.

[5] Ishikawa H, Mendoza O, Nishikawa Y, Maruyama Y, Umeda M. Thermal characteristics of lithium ion secondary cells in high temperature environments using an accelerating rate calorimeter. Journal of Renewable and Sustainable Energy. 2013;5:043122.

[6] Smith J, Hinterberger M, Hable P, Koehler J. Simulative method for determining the optimal operating conditions for a cooling plate for lithium-ion battery cell modules. Journal of Power Sources. 2014;267:784-92.

[7] Pesaran AA. Battery thermal management in EV and HEVs: issues and solutions. Battery Man. 2001;43:34-49.

[8] Sefidan AM, Sojoudi A, Saha SC. Nanofluid-based cooling of cylindrical lithium-ion battery packs employing forced air flow. International Journal of Thermal Sciences. 2017;117:44-58.

[9] Angayarkanni S, Philip J. Effect of nanoparticles aggregation on thermal and electrical conductivities of nanofluids. Journal of Nanofluids. 2014;3:17-25.

[10] Yang X-H, Tan S-C, Liu J. Thermal management of Li-ion battery with liquid metal. Energy conversion and management. 2016;117:577-85.

[11] Jarrett A, Kim IY. Influence of operating conditions on the optimum design of electric vehicle battery cooling plates. Journal of Power sources. 2014;245:644-55.

[12] Panchal S, Khasow R, Dincer I, Agelin-Chaab M, Fraser R, Fowler M. Thermal design and simulation of mini-channel cold plate for water cooled large sized prismatic lithium-ion battery. Applied Thermal Engineering. 2017;122:80-90.

[13] Karimi G, Dehghan A. Thermal management analysis of a lithium-ion battery pack using flow network approach. International Journal of Mechanical Engineering and Mechatronics. 2012;1:88-94.

[14] Hao Y, Li-Fang W, Li-Ye W. Battery thermal management system with liquid cooling and heating in electric vehicles. Journal of Automotive Safety and Energy. 2012;3:371.

[15] Wang J, Lu S, Wang Y, Ni Y, Zhang S. Novel investigation strategy for mini‐channel liquid‐cooled battery thermal management system. International Journal of Energy Research. 2020;44:1971-85.

[16] Qian Z, Li Y, Rao Z. Thermal performance of lithium-ion battery thermal management system by using mini-channel cooling. Energy Conversion and Management. 2016;126:622-31.

[17] Liu H-l, Shi H-b, Shen H, Xie G. The performance management of a Li-ion battery by using tree-like mini-channel heat sinks: Experimental and numerical optimization. Energy. 2019;189:116150.

[18] Huo Y, Rao Z, Liu X, Zhao J. Investigation of power battery thermal management by using mini-channel cold plate. Energy Conversion and Management. 2015;89:387-95.

[19] Chen K, Chen Y, Song M, Wang S. Multi‐parameter structure design of parallel mini‐channel cold plate for battery thermal management. International Journal of Energy Research. 2020;44:4321-34.

[20] Lee Y-J, Lee P-S, Chou S-K. Hot spot mitigating with oblique finned microchannel heat sink. ASME International Mechanical Engineering Congress and Exposition2010. p. 167-74.

[21] Jin L, Lee P, Kong X, Fan Y, Chou S. Ultra-thin minichannel LCP for EV battery thermal management.

Applied energy. 2014;113:1786-94.

[22] Om NI, Zulkifli R, Gunnasegaran P. Influence of the oblique fin arrangement on the fluid flow and thermal performance of liquid cold plate. Case studies in thermal engineering. 2018;12:717-27.

[23] Mohammed AH, Esmaeeli R, Aliniagerdroudbari H, Alhadri M, Hashemi SR, Nadkarni G, et al. Dual-purpose cooling plate for thermal management of prismatic lithium-ion batteries during normal operation and thermal runaway. Applied Thermal Engineering. 2019;160:114106.

[24] Fu J, Xu X, Li R. Battery module thermal management based on liquid cold plate with heat transfer enhanced fin. International Journal of Energy Research. 2019;43:4312-21.

[25] Xu X, Tong G, Li R. Numerical study and optimizing on cold plate splitter for lithium battery thermal management system. Applied Thermal Engineering. 2020;167:114787.

[26] Liang C, Rao Y, Luo J, Luo X. Experimental and Numerical Study of Turbulent Flow and Heat Transfer in a Wedge-shaped Channel with Guiding Pin Fins for Turbine Blade Trailing Edge Cooling. International Journal of Heat and Mass Transfer. 2021;178:121590.

[27] Zhang P, Rao Y, Xie Y, Zhang M. Turbulent flow structure and heat transfer mechanisms over surface vortex structures of micro V-shaped ribs and dimples. International Journal of Heat and Mass Transfer. 2021;178:121611.

[28] Chi Z, Kan R, Ren J, Jiang H. Experimental and numerical study of the anti-crossflows impingement cooling structure. International Journal of Heat and Mass Transfer. 2013;64:567-80.

[29] Rao Z, Huo Y, Liu X, Zhang G. Experimental investigation of battery thermal management system for electric vehicle based on paraffin/copper foam. Journal of the Energy Institute. 2015;88:241-6.